Rare Metal Materials and Engineering
Volume 51, Issue 12, December 2022
Available online at www.rmme.ac.cn

Science Press

Cite this article as: Dai Xiaojun, Yang Xirong, Wang Chang, et al. Effects of Zn on Microstructure, Mechanical Properties and Corrosion Behavior of Mg-Sr Alloy[J]. Rare Metal Materials and Engineering, 2022, 51(12): 4421-4428.

ARTICLE

Effects of Zn on Microstructure, Mechanical Properties and Corrosion Behavior of Mg-Sr Alloy

Dai Xiaojun[1], Yang Xirong[1], Wang Chang[2], Li Xiaocheng[2], Yu Sen[2], Yu Zhentao[1,2,3]

[1] School of Metallurgical Engineering, Xi'an University of Architecture and Technology, Xi'an 710055, China; [2] Shaanxi Key Laboratory of Biomedical Metal Materials, Northwest Institute for Nonferrous Metal Research, Xi'an 710016, China; [3] Institute of Advanced Wear & Corrosion Resistant and Functional Materials, Jinan University, Guangzhou 511486, China

Abstract: Magnesium-strontium series alloys are one of the most prospective biodegradable metal materials, which perform well in biocompatibility because strontium has the function of promoting osteogenesis and regeneration. But the shortcomings of magnesium alloys such as inadequate strength and rapid degradation rate still exist. In the present study, an appropriate amount of human nutrient element zinc was added into Mg-2Sr alloy. Since the solid solution effect of zinc in the alloy can refine the grains, the strength and plasticity of Mg-2Sr alloy are improved. Results show that the Mg-2Sr-2Zn alloy has better corrosion resistance during the degradation processing. The corrosion protection layer is relatively dense, which hinders the penetration of chlorine ions in the simulated body fluid during the soaking process.

Key words: magnesium-strontium alloy; zinc element; mechanical property; corrosion resistance

In the past few years, magnesium and its alloys have attracted extensive attention as biodegradable materials due to their excellent biocompatibilityle, elastic modulus close to human bone and degradability in physiological environment. Magnesium can avoid the stress shielding effect and promote the healing of bone for bone implants[1-3]. It can also reduce the risk of restenosis by self-degradation after a period of positive remodeling with stent support and drug treatment in the stenosis vessels for cardiovascular stent application[4,5]. It should be noted that the metal ions released after the degradation of magnesium alloy can cause biological reactions in surrounding tissues. Inappropriate elements may produce cytotoxicity and even cause the death of cells in nearby tissues[6,7]. At present, the research of industrial magnesium alloy system is mainly focused on Mg-RE and Mg-Al magnesium alloys, but studies have found that Al is cytotoxicity and associated with Alzheimer's disease. The toxicity of many rare earth elements is unclear[8,9]. Nutrient element alloying is one of the latest and most effective methods to improve mechanical properties of biological magnesium alloy from the perspective of biocompatibility. It is better to choose the elements that exist in the human body, especially the essential elements in the human body[10,11]. Based on this design principle, a series of binary alloys have been developed, including Mg-Ca[12], Mg-Zn[13,14], Mg-Sr[15,16], Mg-Mn[17], Mg-Sn[18,19], Mg-Li[20], etc.

Among the as-studied alloy systems, Mg-Sr alloys have been considered as a potential biodegradable materials used in orthopedic surgery mainly due to the effect of Sr on stimulating bone formation and decrease of bone resorption. Strontium is a trace metal found in the human body and 99% of it is found in bones. An adult male has 140 mg of strontium and the mean daily intake is 2 mg. Because strontium has a stimulating effect on bone formation, oral strontium salt can be used to treat osteoporotic patients with increasing bone mass and reducing the incidence of fracture[21,22]. Zhao et al[23] conducted immersion and electro-chemical tests and found that the extruded Mg-0.5Sr alloy has good corrosion resistance and no cytotoxicity to cells through cytotoxicity tests. Gu et al[21] researched that the rolled Mg-2Sr alloy has grade I cytotoxicity and increased ALP activity through in vitro cell experiments. The results of animal experiments

Received date: January 12, 2022
Foundation item: Innovation Chain of Key Science and Technology Industry in Shaanxi Province (2019ZDLGY05-06, 2020ZDLGY13-05)
Corresponding author: Yu Zhentao, Ph. D., Professor, Northwest Institute for Nonferrous Metal Research, Xi'an 710016, P. R. China, Tel: 0086-29-86264213, E-mail: yzt@c-nin.com

showed that the rolled Mg-2Sr alloy can promote bone mineralization and new bone formation around the implant without causing any obvious adverse reactions. Bornapour et al[24] found that the implantation of Mg-0.5Sr alloy in animal blood vessels does not cause thrombosis within three weeks. Moreover, Sr-substituted HA layer forms on the surface of Mg-0.5Sr alloy during SBF biological corrosion and it improves the corrosion resistance of magnesium alloy under physiological conditions and can promote the growth, proliferation and healing of cells around the bone implant. It is expected that Mg-Sr has good biocompatibility and can be used as a bone implant material.

The Mg-Sr binary alloys perform favorable biological compatibility, but their mechanical properties and corrosion resistance are difficult to meet the design requirements. The previous research has shown that adding a small amount of Zn has a significant effect on refining the microstructure of Mg alloy, which is beneficial to improve the mechanical properties and corrosion resistance of Mg alloy. Moreover, the implants of magnesium alloy with Zn element do not produce harmful corrosion products during the degradation. As an essential trace element, Zn is involved in the development and growth of human somatic cells, gene expression, immune system, nervous system and other physiological processes[14,25]. Zhang[26] studied the effect of solid solution precipitation strengthening of Zn element on Mg-6Zn alloy, which significantly refined the grain and improved the yield strength and ultimate tensile strength of the alloy. Song et al[27] researched that the mechanical properties of Mg-0.5wt% Ca alloy can be improved obviously by adding a small amount of Zn element. Brar et al[28] studied the effect of different Zn content on the mechanical properties and corrosion resistance of Mg-0.5Sr and found that the addition of Zn can improve the mechanical properties and ultimate strength of the alloy. Cai et al[14] found that in binary Mg-Zn alloy, the strength of the alloy and the corrosion resistance increase with the increase in Zn content. Chen et al[29] researched that adding 1wt% Zn into Mg-2Sr alloy can significantly improve corrosion resistance and biocompatibility of the alloy.

At present, it is rarely reported that the mechanical properties and corrosion resistance of Mg-2Sr can be adjusted by adding different contents of other elements. In this work, the properties of Mg-2Sr alloys with different contents of Zn were investigated.

1 Experiment

The cast Mg-2Sr-*x*Zn ingots used in this study were prepared by vacuum melting method. The pure Mg (99.99%), Mg-20%Sr master alloy and pure Zn (99.99%) were melted in a high purity graphite crucible under a vacuum condition. After heating at 700 °C for 30 min, the melt was poured into a steel mold preheated to 280 ° C. The actual chemical compositions of three cast alloys were analyzed by inductively coupled plasma atomic emission spectrometry (ICP-MS, Optima 2000DV), as shown in Table 1.

The sample with a dimension of 8 mm was used for microstructure observation and composition analysis, which was first cut from the ingot by wire cutting, then coarsely ground with SiC grinding to a grit of 2000#, and then fine-ground with SiC grinding to a grit of 4000#, and finally polished with SiC polishing fluid. Then the sample was etched with a mixed solution of picric acid (0.5 g), acetic acid (5 mL), ethanol (25 mL) and water (10 mL) to obtain a clear grain boundary. The microstructure was characterized by scanning electron microscopy (SEM), energy dispersive spectroscopy (EDS) and X-ray diffraction (XRD). Grain size was measured using the linear intercept method described in ASTM standard E112-12.

Table 1 Actual chemical compositions of as-cast Mg-2Sr-*x*Zn magnesium alloys (wt%)

Alloy	Mg-2Sr	Mg-2Sr-Zn	Mg-2Sr-2Zn	Mg-2Sr-4Zn
Mg	Bal.	Bal.	Bal.	Bal.
Sr	1.89	1.88	1.91	1.87
Zn	-	0.93	1.88	3.86
Al	0.012	0.01	0.014	0.011
Cu	≤0.001	≤0.001	≤0.001	≤0.001
Fe	0.0004	0.0003	0.0003	0.0004
Ni	≤0.0001	≤0.0001	≤0.0001	≤0.0001

The tensile test at room temperature was conducted on the universal experimental machine with INSTRON5982, and the tensile direction was consistent with the casting direction. The standard for the test was GB/T228.1-2010 and three samples were tested for each state and the mean value was used to evaluate the tensile mechanism. The fracture morphology of samples was observed using a scanning electron microscope (SEM, JMS-6460).

The electrochemical performance tests of Mg-2Sr-*x*Zn samples were carried out in simulated body fluid (SBF) with a pH of 7.4 by the ZENNIUMTM6 electrochemical analyzer. The SBF was composed of 8.035 g/L NaCl, 0.355 g/L $NaHCO_3$, 0.225 g/L KCl, 0.231 g/L K_2HPO_4·3H2O, 0.311 g/L $MgCl_2·6H_2O$, 39 mL/L (1 mol/L) HCl, 0.292 g/L $CaCl_2$, 0.072 g/L Na_2SO_4, and 6.118 g/L $(CH_2OH)_3CNH_2$. The electrochemical tests adopted three electrode equipment, with the control or treated samples as a working electrode, the saturated calomel electrode as a reference electrode and the platinum plate electrode as a counter electrode. The area of the samples exposed to SBF was about 1 cm^2. Both the potentiodynamic polarization test and electrochemical impedance spectroscopy (EIS) tests were conducted at a stable open-circuit potential. The scan rate of the potentiodynamic polarization test was 2 mV/s. EIS was carried out at a sinusoidal potential of 5 mV in the frequency range from 10^{-2} Hz to 105 Hz. The tests results and corrosion mechanism were fitted by the software Zsimpwin 3.60. Each test was conducted three times. After the tests, the samples were dried at room temperature.

The immersion tests were also carried out in SBF solution at 37 °C according to ASTM-G31-72 standard. The ratio of

sample area to SBF solution was 1 cm^2: 20 mL. After immersion for 10 d, the samples were removed from SBF solution, gently rinsed with distilled water and dried in air. The corrosion surface morphology and chemical composition of corrosion products were measured by scanning electron microscope (SEM, JMS-6460).

2 Results

2.1 Microstructure characterization

Fig. 1 shows the SEM images of Mg-2Sr-*x*Zn magnesium alloy with different contents of Zn element. It can be seen that the grain homogenization of the alloy is obvious through the addition of Zn element. With the increase in Zn content, the grains of Mg-2Sr-*x*Zn alloy are significantly refined. Compared with Mg-2Sr magnesium alloy, the Mg-2Sr-2Zn has the most obvious grain refinement effect among all the magnesium alloys, with an average grain size of 33 μm. The second phase at the grain boundary of Mg-2Sr magnesium alloy is coarse, but the second phase at the grain boundary is refined and evenly distributed by the addition of Zn element. However, with the further addition of Zn element, the grains of Mg-2Sr-4Zn grow up and the proportion of the second phase at grain boundary increases.

Fig. 2 shows the XRD patterns of Mg-2Sr-*x*Zn magnesium alloys with different Zn contents. Most of the diffraction peaks with relatively strong intensities can be identified as the complete spectrum of α-Mg phase. The data show that all alloys contain α-Mg and $Mg_{17}Sr_2$ phases, but the MgZn phase only appears in Mg-2Sr-4Zn magnesium alloy. Compared with the case in Mg-2Sr-2Zn magnesium alloy, the formation of MgZn phase occurs at the grain boundary in Mg-2Sr-4Zn .

2.2 Mechanical property

Fig. 3 shows the tensile test results of Mg-2Sr-*x*Zn magnesium alloy with different Zn contents at room temperature. With the increase in Zn content, the strength of Mg-2Sr-*x*Zn magnesium alloy continuously increases, and the elongation shows a similar trend, but there is an obvious deterioration when the Zn content increases to 4wt%. This indicates that the mechanical properties of the alloys can be significantly affected by the addition of a small amount of Zn. The elongation of Mg-2Sr-2Zn alloy reaches the peak value, so that the comprehensive properties are improved most significantly. The YS, UTS and elongation increase from 119 MPa, 130 MPa and 3.2% to 181 MPa, 212 MPa and 8.1%, respectively. However, with the further addition of Zn element, the strength of Mg-2Sr-4Zn magnesium alloy reaches the maximum, but the ductility is worse than that of Mg-2Sr-2Zn magnesium alloy. Therefore, the experimental specimen with the addition of 2wt% Zn presents the best strength and ductility performance compared with other specimens.

Cleavage fracture, quasi-cleavage fracture and intergranular fracture are the main fracture modes of magnesium alloys. Fig. 4 shows the SEM fracture morphologies of Mg-2Sr-*x*Zn magnesium alloy tensile sample at room temperature. It can be seen that the fracture mode of all the alloys is mainly intergranular fracture, which is a typical brittle fracture. However, with the addition of Zn element, the grain size of the alloy is significantly reduced, and the crack requires more energy in the process of propagation, which is favorable to higher strength and plasticity. The fracture morphology of Mg-2Sr-Zn and Mg-2Sr-2Zn magnesium alloys shows a small number of cleavage planes, indicating that an appropriate amount of Zn is beneficial to improve the plasticity of the alloys. However, excessive Zn elements leads to deterioration of the plasticity of the alloy, and the fracture mode of Mg-2Sr-4Zn alloy is completely intergranular fracture. A large amount of the second phases are distributed on the fracture surface of all the samples, especially the Mg-2Sr-4Zn magnesium alloy.

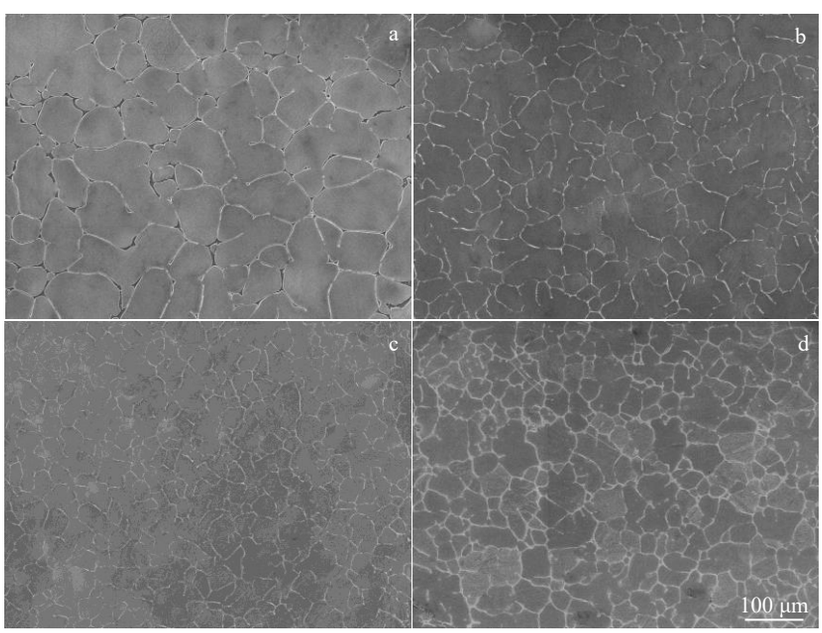

Fig.1 SEM images of as-cast Mg-2Sr-*x*Zn magnesium alloy: (a) Mg-2Sr, (b) Mg-2Sr-1Zn, (c) Mg-2Sr-2Zn, and (d) Mg-2Sr-4Zn

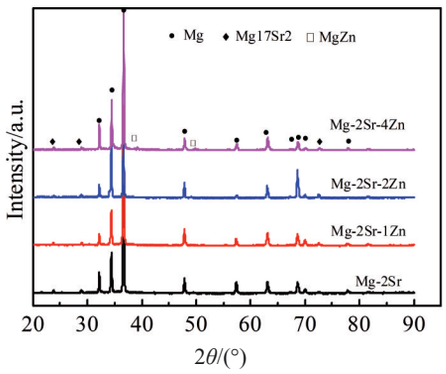

Fig.2 XRD patterns of as-cast Mg-2Sr-*x*Zn alloys

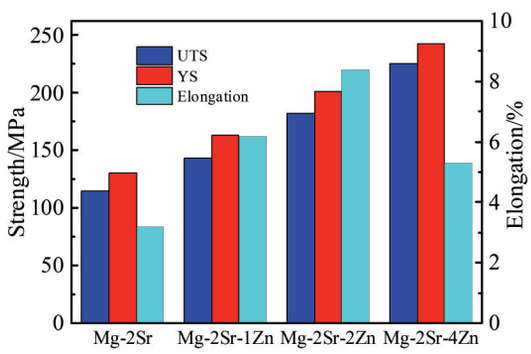

Fig.3 Mechanical properties of as-cast Mg-2Sr-*x*Zn alloys

2.3 Experimental tests in SBF

The early degradation behavior of Mg-2Sr-*x*Zn magnesium alloy was studied using a soaking experiment in SBF. The pH value of the solution was measured during immersion to reflect the early degradation of the alloy. Fig. 5 shows the pH change curve of SBF solution during 144 h immersion. During the early soaking period of 0~36 h, the soaking pH value of different samples increases sharply from 7.4 to 8.3~8.88. Then the pH gradually increases during the subsequent immersion process, mainly due to the accumulation of early corrosion products, resulting in the formation of oxide film on the alloy surface. At the later soaking period between 96 h to 144 h, the pH value of the soaking sample increases slowly and tends to be stable. After soaking in SBF for 144 h, the minimum pH value of Mg-2Zn-2Sr alloy is 9.15, showing the best corrosion resistance.

Fig.6 shows the dynamic potential polarization curve of Mg-2Sr-*x*Zn magnesium alloy with different Zn contents in Hank's solution. Table 2 lists the corrosion potential and corrosion current density of the dynamic potential polarization curve of the as-cast Mg-2Sr-*x*Zn alloy as well as the related corrosion rate. By adding an appropriate amount of zinc, the corrosion potential (E_{corr}) of Mg-2Sr-*x*Zn magnesium alloy increases obviously, but excessive zinc leads to the decrease in corrosion potential. The corrosion current density (i_{corr}) and related corrosion rate (R_i) of alloys are in the order of Mg-2Sr-2Zn<Mg-2Sr-Zn<Mg-2Sr-4Zn<Mg-2Sr.

Fig. 7a shows the electrochemical impedance spectroscopy (EIS) spectra of Mg-2Sr-*x*Zn magnesium alloys measured at open circuit potential. The EIS spectra of the four magnesium alloys are all composed of two rings: the capacitance ring in the high frequency region (HF) and the capacitance ring in the middle frequency region (MF). According to the same shape and different radii of impedance spectrum, it can be analyzed that the four magnesium alloys have the same corrosion mechanism and different corrosion rates. The Mg-2Sr-2Zn magnesium alloy has the largest impedance radius, indicating the best corrosion resistance.

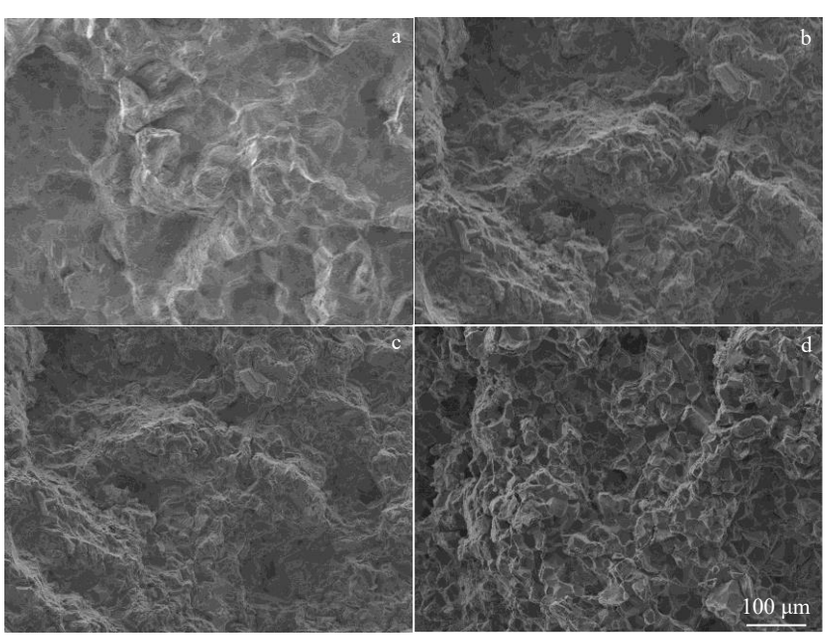

Fig.4 SEM fracture morphologies of tensile specimen at room temperature of as-cast Mg-2Sr-*x*Zn alloys: (a) Mg-2Sr, (b) Mg-2Sr-1Zn, (c) Mg-2Sr-2Zn, and (d) Mg-2Sr-4Zn

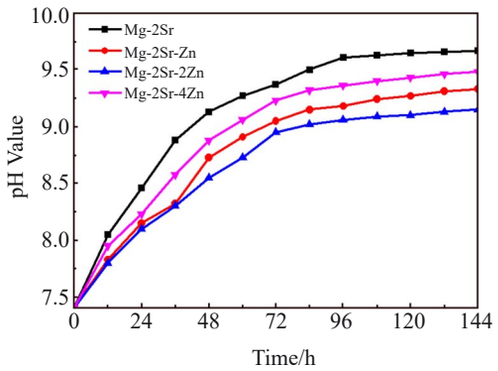

Fig.5 pH change curve of SBF solution during 144 h immersion of as-cast Mg-2Sr-*x*Zn magnesium alloys

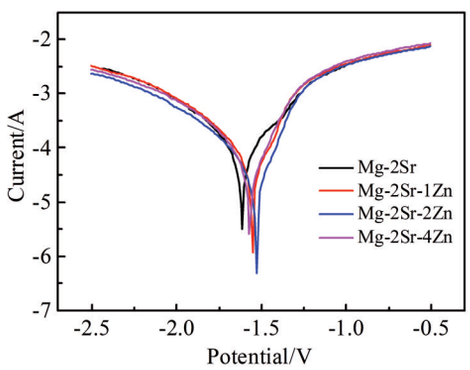

Fig.6 Dynamic potential polarization curves of as-cast Mg-2Sr-*x*Zn magnesium alloys

Table 2 Values measured from mass loss and the polarization curves for as-cast Mg-2Sr-*x*Zn magnesium alloys in SBF

Alloy	E_{corr}/V	i_{corr}/μA·cm^{-2}	R_t/mm·a^{-1}
Mg-2Sr	-1.612	242±10.3	5.53±0.05
Mg-2Sr-Zn	-1.561	113±6.2	2.55±0.03
Mg-2Sr-2Zn	-1.533	81±5.6	1.83±0.02
Mg-2Sr-4Zn	-1.582	200±6.5	4.58±0.03

Fig. 8 shows the mass loss rate of Mg-2Sr-*x*Zn magnesium alloy with different Zn contents soaked in Hank's solution for 240 h. It can be seen that the addition of Zn alloy contributes to the improvement of the corrosion resistance of Mg-2Sr-*x*Zn, but when the addition content of Zn reaches a certain level, excessive Zn will lead to the decrease in the corrosion resistance. The corrosion rate of Mg-2Sr-*x*Zn alloy calculated by mass loss method decreases from 6.63 mm/a to 2.21 mm/a with the increase in Zn content from 0wt% to 2wt%, and increases to 4.88 mm/a with the increase of Zn content to 4wt%. These results are consistent with pH tests, indicating that Mg-2Sr-2Zn magnesium alloy has the best corrosion resistance in all soaking samples.

Fig. 9 shows the surface morphologies of Mg-2Sr-*x*Zn magnesium alloys observed by SEM after soaking in SBF for 240 h. It can be seen that the surface of all samples is covered

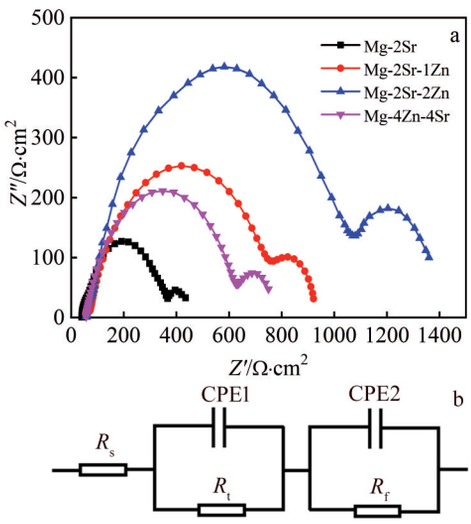

Fig.7 Nyquist plots for as-cast Mg-2Sr-*x*Zn magnesium alloys after soaking in SBF for 1 h (a) and corresponding equivalent circuit (b)

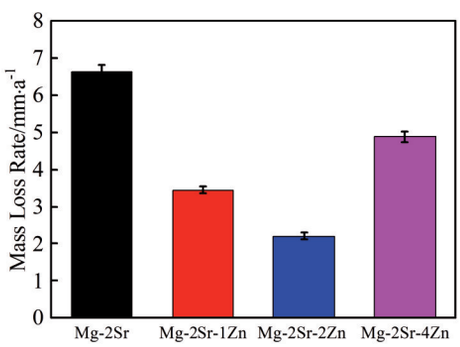

Fig.8 Mass loss rate of as-cast Mg-2Sr-*x*Zn alloy soaked in Hank's solution for 240 h

with corrosion product film after immersion. The oxide film on the surface of Mg-2Sr magnesium alloy is loose that is more likely to cause more serious local corrosion in the subsequent immersion process. With the addition of Zn element, the oxide film on the surface of Mg-2Sr-*x*Zn alloys becomes denser and shows better corrosion resistance. The oxide film generated on the surface of alloy is relatively dense, which can better impede the possibility of subsequent serious corrosion and ensure the integrity of the sample. However, with the increase in Zn element to 4wt%, more cracks occur on the surface of Mg-2Sr-4Zn, resulting in poor density.

3 Discussion

The microstructure, mechanical properties and corrosion behavior of Mg-2Sr alloys added with different Zn contents (0wt%~4wt%) were investigated. As can be seen from Fig. 1, the addition of an appropriate amount of Zn element is beneficial to grain refinement and distribution homogenization of the second phase. Due to the low solid solubility of

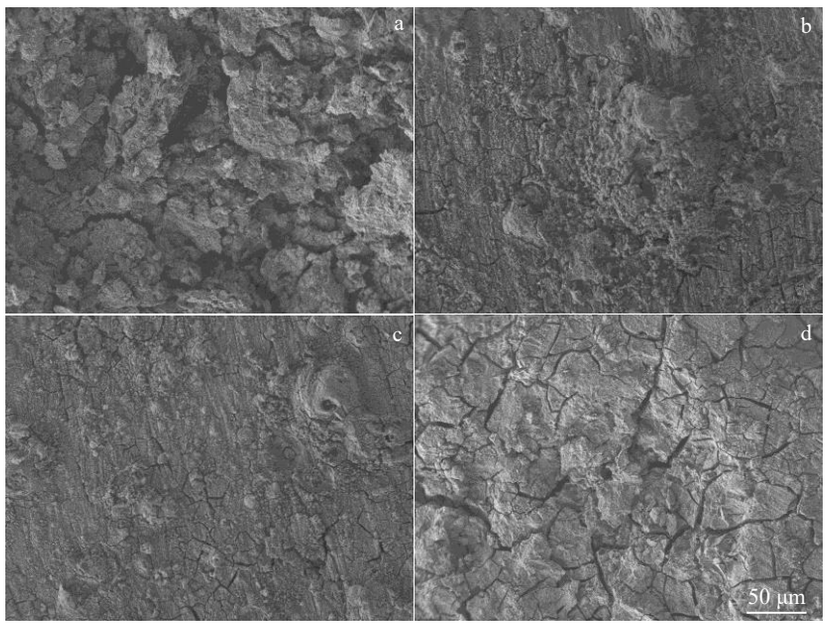

Fig.9 SEM surface morphologies of as-cast Mg-2Sr-*x*Zn magnesium alloy after soaking in SBF for 240 h: (a) Mg-2Sr, (b) Mg-2Sr-1Zn, (c) Mg-2Sr-2Zn, and (d) Mg-2Sr-4Zn

Sr solute in α-Mg matrix (about 0.11wt%), Sr mainly exists in the form of $Mg_{17}Sr_2$ in the second phase[30,31]. The solid solubility of Zn solute in α-Mg matrix is relatively high (about 1.6wt%), and the amount of Zn element mainly exists in the form of solid solution, while the excess Zn element mainly exists in the form of the second phase of MgZn[14,32]. It can be determined from the element distribution diagram in Fig. 10 that most element Sr is distributed at grain boundaries in the Mg-2Sr-2Zn magnesium alloy, while element Zn is partially distributed in grains. Although the volume fraction of secondary phase is generally reduced by a lower percentage of alloying elements, the Zn/Sr atomic ratio can play a critical role in mechanical and corrosion properties of the Mg-Zn-Sr alloys. Li et al[33] also suggested that the formation of the $Mg_xZn_ySr_z$ is strongly related to the Zn content in the Mg-Zn-Sr alloys. The reason why the addition of Zn leads to the decrease in grain size is that the segregation of Zn will lead to the formation of a dense component undercooling zone in the diffusion layer at the front of the solid-liquid interface. When the undercooling degree is large enough, the balance of the interface will be destroyed and dendrites will be generated. With the increase in Zn content, the potential nucleation particles in the supercooled region of the component are activated, which promotes the nucleation of α-Mg matrix, and eventually leads to grain size refinement[34].

The addition of Zn is beneficial to grain refinement, which can improve the uniformity of deformation and reduce the stress concentration. According to the Hall-Petch formula, grain refinement provides more grain boundaries, leading to an increase in strength[35]. A proper amount of Zn atoms dissolved into Mg matrix also produces solid solution strengthening effect. The increase in strength can be attributed to grain refining and precipitation strengthening effect of Zn element. Refining grain improves deformation compatibility and plasticity. In addition, the casting defects, relative density, strength and plasticity of Mg-Zn alloy are improved by grain refinement[36]. When Zn is added further, the precipitation of MgZn greatly increases the possibility of crack source and leads to the decrease in alloy plasticity[37].

It has been reported that the addition of Zn to magnesium can improve the corrosion potential of Mg, which is consistent with the results in this study[38]. As a cathode, the secondary phase is easy to form a micro couple with Mg matrix, which accelerates the corrosion. The synergistic effect of grain

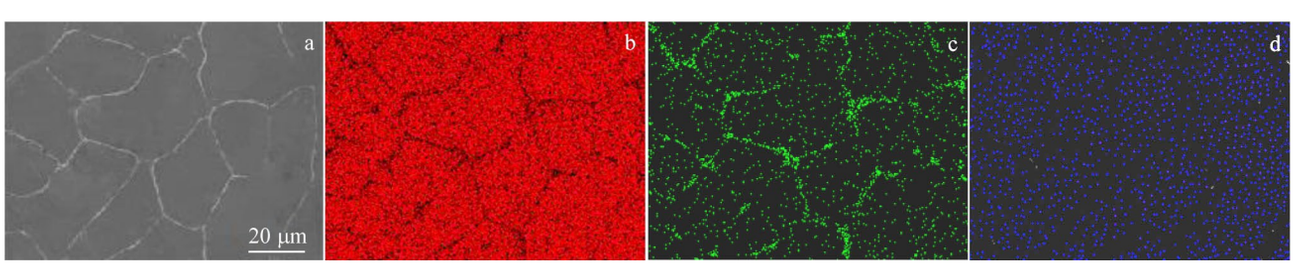

Fig.10 SEM image of Mg-2Sr-2Zn magnesium alloy (a) and corresponding EDS mappings of Mg (b), Sr (c), and Zn (d)

refinement and secondary phase formation results in the change of corrosion resistance of the alloys with different Zn contents[10,37]. With the increase in Zn content to more than 4wt%, the number of MgZn intermetallic phases in the matrix increases rapidly, forming a continuous network structure and more anode-cathode sites. Therefore, more galvanic corrosion may occur at these locations, resulting in rapid corrosion[21].

In this study, the impedance spectra of all magnesium alloys are composed of two rings: capacitance ring in the high frequency region and capacitance ring in the middle frequency region, as shown in Fig. 7a. Generally speaking, the high frequency capacitor circuit is attributed to the relaxation process of electrochemical reaction impedance corresponding to the dissolution of Mg and electric double layer capacitance (C_{dl}) between the magnesium surface dissolution and the interface of the corrosive medium, while the medium frequency capacitor circuit is related to the formation of oxide film during the corrosion process[14,39]. The Nyquist plots of Mg-2Sr-*x*Zn alloys can be interpreted using the equivalent circuit shown in Fig. 7b. According to the shape of impedance spectrum, the electrode reaction process related to the selection of high frequency capacitor circuit can be described by a parallel circuit consisting of capacitor CPE1 and resistor R_t. The intermediate frequency capacitor circuit is described by the parallel circuit composed of capacitor CPE2 and resistor R_f. R_t is inversely proportional to the exchange current density, that is, the larger the R_t, the slower the corrosion rate. According to Nyquist figure, R_t from low to high is in the order of Mg-2Sr (385 cm^2), Mg-2Sr-4Zn (615 cm^2), Mg-2Sr-1Zn (986 cm^2) and Mg-2Sr-2Zn (1352 cm^2).

When the immersion corrosion of Mg-2Sr-*x*Zn alloy occurs in SBF, the microelectrical corrosion occurs between the Mg matrix and the second phase. The anodic reaction converts Mg to Mg^{2+} ions and the cathodic reaction converts H_2O to OH^-, resulting in $Mg(OH)_2$ accumulated on the surface of the sample and gradually forming a protective corrosion film[40,41]. The following reactions give the corrosion reactions of magnesium in Cl^--containing solution[10]:

$$Mg(s)+2H_2O \rightarrow Mg(OH)_2+H_2\uparrow$$

$$Mg(s)+2Cl^-(aq) \rightarrow MgCl_2$$

$$Mg(OH)_2+2Cl^- \rightarrow MgCl_2$$

The addition of different contents of Zn will lead to different degradation rates of magnesium alloys. Magnesium alloys with better corrosion resistance have slower corrosion at the initial stage of degradation, and less H_2 is precipitated on the surface, which is more conducive to the formation of $Mg(OH)_2$[42,43]. The thick and complete corrosion product layer reduces the reaction rate of magnesium alloy in SBF solution, thus improving its corrosion resistance[44]. $Zn(OH)_2$ is produced during the addition of Zn element, which can improve the compactness of the corrosion products layers[45,46]. Therefore, different alloys have different pH values and H_2 formation amounts. Although corrosion layer has a certain protective effect on alloy corrosion, chloridion ions in SBF will continue to react with the matrix through the corrosion product layer, and the pH value of the solution will continue to increase[16].

The corrosion rate of magnesium alloys is closely related to the microstructure, and the grain size and grain boundary precipitates are important factors affecting the corrosion rate[28,47]. Grain refinement contributes to the formation of passivation layer on the surface of magnesium alloy to improve the corrosion resistance of magnesium alloy, but on the other hand, excessive second phase strengthens the galvanic corrosion between magnesium matrix and the second phase, thus reducing the corrosion resistance of the alloy[47]. Cai et al[14] believed that the refinement of the second phase of magnesium alloy will also improve its corrosion resistance and reduce the galvanic corrosion between the matrix and the second phase. However, the second phase MgZn is formed at the grain boundary by adding excess Zn element, resulting in increased microgalvanic corrosion to α-Mg matrix, thus reducing the corrosion resistance of Mg-2Sr-*x*Zn magnesium alloy and accelerating its corrosion rate.

4 Conclusions

1) The microstructure, mechanical properties and corrosion resistance of Mg-2Sr-*x*Zn (*x*=0, 1, 2, 4, wt%) alloys are studied, and the content of Zn in the alloy leads to different outcomes.

2) The Mg-2Sr-2Zn magnesium alloy performs excellent property. An appropriate amount of Zn (2wt%) helps to refine the grain and plays a role in solid solution enhancement without producing additional second phase. This method is beneficial to improve the plasticity and corrosion resistance of the Mg-2Sr-*x*Zn magnesium alloys.

3) Excessive Zn element will lead to the formation of MgZn phase, which deteriorates the plasticity of the alloy and intensifies the microgalvanic corrosion between the matrix and the second phase, resulting in the accelerated corrosion rate of the Mg-2Sr-*x*Zn magnesium alloys.

References

1 Liu Y, Zheng Y, Chen X H *et al. Advanced Functional Materials*[J], 2019, 29(18): 1 805 402

2 Liu J, Bian D, Zheng Y *et al. Acta Biomaterialia*[J], 2020, 102: 508

3 Kraus T, Fischerauer S F, Hänzi A C *et al. Acta Biomaterialia*[J], 2012, 8(3): 1230

4 Mei D, Lamaka S V, Lu X *et al. Corrosion Science*[J], 2020, 171: 108 722

5 Gonzalez J, Hou R Q, Nidadavolu E P S *et al. Bioactive Materials*[J], 2018, 3(2): 174

6 Sunil B R, Kumar T S S, Chakkingal U *et al. Materials Science and Engineering C*[J], 2016, 59: 356

7 Wan Y, Xiong G, Luo H *et al. Materials & Design*[J], 2008, 29(10): 2034

8 Xiong P, Jia Z, Li M *et al. ACS Biomaterials Science & Engineering*[J], 2018, 4(9): 3163

9 Liu J, Zheng Y, Bi Y *et al. Materials Letters*[J], 2017, 205: 87

10 Zhao C, Chen X, Pan F *et al. Journal of Materials Science & Technology*[J], 2019, 35(1): 142

11 Dxab C, Fan Y, Yzb C *et al. Bioactive Materials*[J], 2021, 6(11): 4186

12 Li Z, Gu X, Lou S *et al. Biomaterials*[J], 2008, 29(10): 1329

13 Zhang S, Zhang X, Zhao C *et al. Acta Biomaterialia*[J], 2010, 6(2): 626

14 Cai S, Lei T, Li N *et al. Materials Science and Engineering C*[J], 2012, 32(8): 2570

15 Bornapour M, Muja N, Shum-Tim D *et al. Acta Biomaterialia*[J], 2013, 9(2): 5319-

16 Zhao C, Pan F, Zhang L *et al. Materials Science and Engineering C*[J], 2017, 70: 1081

17 Gu X, Zheng Y, Cheng Y *et al. Biomaterials*[J], 2009, 30(4): 484

18 Dong C, Ren Y P, Yun G *et al. Transactions of Nonferrous Metals Society of China*[J], 2010, 20(7): 1321

19 Zhao C, Pan F, Zhao S *et al. Materials & Design*[J], 2015, 70: 60

20 Xu W, Birbilis N, Sha G *et al. Nature Materials*[J], 2015, 14(12): 1229

21 Gu X N , Xie X H , Li N *et al. Acta Biomaterialia*[J], 2012, 8(6): 2360

22 Wang Y, Tie D, Guan R *et al*. *Journal of the Mechanical Behavior of Biomedical Materials*[J], 2018, 77: 47

23 Zhao C, Pan F, Zhang L *et al. Materials Science and Engineering C*[J], 2017, 70: 1081

24 Bornapour M , Muja N , Shum-Tim D *et al. Acta Biomaterialia*[J], 2013, 9(2): 5319

25 Chen Y, Xu Z, Smith C *et al. Acta Biomaterialia*[J], 2014, 10(11): 4561

26 Zhang S, Zhang X, Zhao C *et al. Acta Biomaterialia*[J], 2010, 6(2): 626

27 Song J, She J, Chen D *et al. Journal of Magnesium and Alloys*[J], 2020, 8(1): 1

28 Brar H S, Wong J, Manuel M V. *Journal of the Mechanical Behavior of Biomedical Materials*[J], 2012, 7: 87

29 Chen K, Xie X, Tang H *et al. Bioactive Materials*[J], 2020, 5(2): 275

30 Bornapour M, Celikin M, Cerruti M *et al. Materials Science and Engineering C*[J], 2014, 35(2): 267

31 Bornapour M , Muja N , Shum-Tim D *et al. Acta Biomaterialia*[J], 2013, 9(2): 5319

32 Kamoto H. *Journal of Phase Equilibria*[J], 1994, 15(1): 129

33 Cipriano A F, Sallee A, Tayoba M *et al. Acta Biomaterialia*[J], 2017, 48: 499

34 Romzi M A F, Alias J, Ramli M I M. *Materials Today: Proceedings*[J], 2022, 48: 1873

35 Wen Y, Guan B, Xin Y *et al. Scripta Materialia*[J], 2022, 210: 114 451

36 Yan H, Chen R S, Han E H. *Materials Science and Engineering A*[J], 2010, 527(15): 3317

37 Zhang H J, Zhang D F, Ma C H *et al. Materials Letters*[J], 2013, 92: 45

38 Meng X, Jiang Z, Zhu S *et al. Journal of Alloys and Compounds*[J], 2020, 838: 155 611

39 Liu M, Uggowitzer P J, Nagasekhar A V *et al. Corrosion Science*[J], 2009, 51(3): 602

40 Lai H, Li J, Li J *et al. Journal of Materials Science: Materials in Medicine*[J], 2018, 29(6): 1

41 Li H, Peng Q, Li X *et al. Materials & Design*[J], 2014, 58: 43

42 Wu Y, He G, Zhang Y *et al. Scientific Reports*[J], 2016, 6(1): 1

43 Atrens A, Johnston S, Shi Z *et al. Scripta Materialia*[J], 2018, 154: 92

44 Zander D, Zumdick N A. *Corrosion Science*[J], 2015, 93: 222

45 Chen M X , Chen J H, Yan H G *et al. Journal of Alloys and Compounds*[J], 2017, 691: 95

46 Gu X, Zheng Y, Zhong S *et al. Biomaterials*[J], 2010, 31(6): 1093

47 Hamu G B, Eliezer D, Wagner L. *Journal of Alloys and Compounds*[J], 2009, 468(1-2): 222

Zn元素对Mg-Sr镁合金显微组织、力学性能及腐蚀行为的影响

代晓军[1]，杨西荣[1]，王　昌[2]，李小成[2]，余　森[2]，于振涛[1,2,3]

(1. 西安建筑科技大学 冶金工程学院，陕西 西安 710055)

(2. 西北有色金属研究院 陕西省医用金属材料重点实验室，陕西 西安 710016)

(3. 暨南大学 先进耐磨蚀及功能材料研究院，广东 广州 511486)

摘　要：镁锶系列镁合金是最有前景的生物可降解金属材料之一。锶具有促进成骨和再生的作用，具有良好的生物相容性。但是镁锶合金具有强度不足、降解快速等缺点。添加适量的人体营养元素Zn在Mg-2Sr合金中，通过锌在镁合金中的固溶作用来细化晶粒以提高Mg-2Sr合金的强度和塑性。在模拟体液浸泡降解过程中，Mg-2Sr-2Zn合金生成的腐蚀保护层较致密，阻碍了浸泡过程中氯离子渗透，从而具有较好的耐蚀性。

关键词：镁锶合金；锌元素；力学性能；抗腐蚀性能

作者简介：代晓军，男，1989年生，博士生，西安建筑科技大学冶金工程学院，陕西 西安 710055，电话：029-86222297，E-mail：296648131@qq.com